Assessing Processing Strategies on Data from Medical Hyperspectral Acquisition Systems

Laura Quintana-Quintana[1*], Carlos Vega[1], Raquel Leon[1], Guillermo V. Socorro-Marrero[1], Samuel Ortega[2,1,3*], Gustavo M. Callico[1]
[1]Research Institute for Applied Microelectronics (IUMA), University of Las Palmas de Gran Canaria (ULPGC), Spain
[2]Norwegian Institute of Food, Fisheries and Aquaculture Research (Nofima), Tromsø, Norway
[3]Department of Mathematics and Statistics, UiT The Arctic University of Norway, Tromsø, Norway
*{lquintana, sortega}@iuma.ulpgc.es

***Abstract*— Hyperspectral imaging (HSI) has gained prominence in medical diagnostics due to its ability to capture and analyse detailed spectral information beyond human visual capabilities. Processing of HSI data is essential to enhance subsequent analysis and ensure the accuracy of results by reducing noise and unwanted artifacts. This paper provides an overview of state-of-the-art processing methods for HSI data, focusing on smoothing, normalization, and spectral derivatives. The efficacy of these methods is evaluated using root mean square error (RMSE) to compare pre-processed data with wavelength reference standard, alongside execution time considerations. Results indicate that certain algorithms, such as smoothing based on moving average, standard normal variate, and first spectral derivatives, yield superior performance across different medical HSI systems. Additionally, combining these processing techniques further improves data fidelity to the wavelength reference standard. Overall, this study offers insights into optimal processing strategies for enhancing the accuracy and reliability of HSI data.**

Keywords*— *hyperspectral imaging, processing methods, smoothing, normalization, spectral derivatives.

I. INTRODUCTION

Hyperspectral (HS) imaging (HSI) is a technique that captures and analyses a portion of the light spectrum in fine detail, often beyond human visual capabilities. This allows for the detection of substances with different spectral signatures. While initially used in remote sensing [1], HSI is increasingly applied in medical contexts for pathology identification, such as breast tumour [2], brain histological samples [3], colon and esophagogastric cancer [4], or skin and lung cancers [5]. After HSI capturing and prior to the development of tissue classification algorithms, HS data is pre-processed to remove non-tissue-related variability (e.g. inhomogeneities in illumination and noise in acquisition systems). The pre-processing algorithms usually aim to enhance subsequent information extraction from the data, such as compensate data according to Lambert-Beer's law or improving classification and regression models.

Traditional works were centred on spectral correction of HSI data. Numerous studies have investigated near-infrared (NIR) spectroscopy pre-processing, highlighting its critical role for subsequent analysis. It has been widely used in chemometrics, a field dedicated to correlating chemical measurements with properties of interest, such as the concentration of specific molecules. In 2009, Rinnan *et al.* published a review of the most common processing techniques for near-infrared spectra [6]. The authors classified pre-processing algorithms into two categories: scatter-correction and spectral derivatives. The theoretical foundations of the algorithms were explained, and a quantitative experiment was performed over near-infrared data of marzipan samples. Root Mean Square Error (RMSE) results indicated that the maximum improvement of any pre-processed model compared to the unprocessed one was approximately 25 %. These findings underline the challenge of identifying the best pre-processing method, mainly due to the impact of incorrect parameter settings, such as window size for smoothing algorithms. Additionally, it is noted that combining processing techniques is common practice, with guidelines typically recommending smoothing before normalization.

Likewise, in 2013, Engel *et al.* reviewed several pre-processing algorithms for chemometric data analysis (e.g. noise removal, base line offset and slope, light scatter, temporal and spectral misalignment, normalization, etc.) [7]. The authors focused on selecting the optimal data-analysis strategy to choose the combination of pre-processing methods that effectively remove artifacts and enhance the necessary information for various data-analysis goals. They explored three main approaches: trial and error based on subsequent analysis results, visual examination for artifacts, and quantifying data quality parameters to assess artifacts. These strategies were tested on a labelled dataset of beers with different alcohol content. Results indicated that choosing an effective pre-processing method, or combination of methods, significantly impacts analysis outcomes, with a variance of over 20 % in model accuracy between the best and worst pre-processing strategies. The study concluded that suboptimal pre-processing can greatly hinder data analysis goals, highlighting the need for a robust, quantitative approach to determine the optimal pre-processing strategy.

Following these lines, in 2004, Ezenarro *et al.* developed a MATLAB® toolbox named ProSpecTool to aid in selecting optimal pre-processing techniques for regression models in infrared (IR) spectroscopy [8]. ProSpecTool addressed the challenge by using objective criteria to filter and iterate pre-processing methods, including the classic set of pre-processing techniques (smoothing, normalization and derivatives) over raw data. The Forages dataset [9] was used as an example and performance evaluation metrics were calculated using pre-processed data. Results indicated that ProSpecTool can produce robust models comparable to those from trial-and-error approaches, but in significantly less time. Authors suggested that ProSpecTool could be an invaluable exploratory tool for IR

2024 27th Euromicro Conference on Digital System Design (DSD) | 979-8-3503-8038-5/24/$31.00 ©2024 IEEE | DOI: 10.1109/DSD64264.2024.00068

2771-2508/24/$31.00 ©2024 IEEE
DOI 10.1109/DSD64264.2024.00068

spectroscopy practitioners, although final model validation and interpretation remain being the responsibility of the analyst. Recently, in 2023, Cozzolino *et al.* provided a broad overview of pre-processing methods for HSI data [10]. The article discussed several pre-processing methods beyond the former explained scatter correction and spectral derivatives algorithms (e.g., dimension reduction, resolution enhancement, geometric correction). As previous authors have concluded, they stated that pre-processing techniques are crucial to ensure the accuracy and reliability of the results by reducing interferences such as noise and unwanted artifacts. They also highlighted the need for iterative evaluation and simplicity in pre-processing techniques.

Other authors have centred their efforts just on removing noise from HS images, since it can disrupt accuracy of HS spectral-spatial feature classification. Singh *et al.* work proposed a new method involving interpolation to recover lost band information [11]. It employs Principal Components Analysis (PCA) [12] and Locality Preserving Projection (LPP) [13] to extract hybrid features, blending local and global spatial data. They tested it on standard datasets (Indian Pines, Salinas, Pavia University, and Kennedy Space Centre) and results showed that the accuracy of the classification increased significantly (313.81 %, 1448.33 % 153.21 % and 139.21 %, respectively) when the proposed framework is blended with state-of-the-art classifiers. Additionally, Bharath Bhushan *et al.* introduced a processing algorithm for band selection in HSI analysis, focused on removing noisy bands [13]. This algorithm calculates average inter-band block-wise correlation coefficients and applies a simple thresholding strategy based on their standard deviation. Validation using AVIRIS data [14] demonstrates its ability to identify noisy and water absorption bands accurately. The algorithm achieves a 94.73 % probability of correctly detecting noisy bands and a 3.18 % probability of false detection. The authors concluded that this processing algorithm successfully eliminates noise, improves band quality, and reduces computation complexity in band selection.

Out of all the spectral data processing documents found in the state-of-the-art, just two of them specifically addressed processing techniques for medical HS data. In 2015, Koprowski introduced a source code that can be freely used for preliminary HS data analysis on MATLAB® and discusses problems encountered when analysing medical HS images [15]. The application facilitates preliminary analysis of HS images, including reading data in various formats, calibration, filtering, and visualization. The graphical user interface and source code are available for download without restrictions, enabling users to modify and utilize them as needed. However, the authors did not investigate the impact of various standard processing methods on medical HS data. Thus, in 2022, Witteveen *et al.* conducted a comparison of different processing algorithms to reduce variations in spectra, caused by external factors, while preserving contrast between tissues with different optical properties [16]. They created a synthetic database by simulating tissue with differences in blood volume fraction, presence of different absorbers, scatter amplitude, and scatter slope. Furthermore, in order to test the methods for clinical validation, two clinical databases were collected (breast [17] and colorectal [18] tumour) in the Visible and Near Infrared (VNIR) and NIR ranges. Then, they analyse several processing algorithms which can be divided into normalization and spectral derivatives. The evaluation metrics included the overlap coefficient, which was calculated over pre-processed data belonging to different classes (e.g. 0.5 % or 2 % of blood volume fraction). They conclude that, overall, normal standardization (SNV), min–max, area under the curve, and single wavelength normalization are the most appropriate methods for processing data intended for the development of a tissue classification algorithm.

After this review of the state-of-the-art, it can be extracted that the current research faces limitations due to the absence of a clear standard for processing medical HS data. This lack of standard hinders the development of precise HSI intraoperative margin assessment techniques needed in medical context (e.g., complete tumour removal while preserving healthy tissue in cancer surgery) [19]. However, these requirements for precision are not as stringent in fields such as agriculture, food science, or chemometrics. Witteveen *et al.* did a review of eight processing algorithms, but only normalization and spectral derivative methods were studied. The aim of this work is to preliminary design a standard for preprocessing HS data from medical HS acquisition systems. State-of-the-art processing methods are going to be assessed, including noise removal techniques (smoothing), intensity misaligns of signals (normalization) and spectral derivatives. Each algorithm will be applied to HS images of a wavelength reference polymer captured using several medical HS systems. Finally, the data resulting from each processing method, or combination of them, will be evaluated against the wavelength reference standard of the material using RMSE, while also considering execution time.

II. Material and Methods

The whole set of medical HS systems included in this work will be described, the spectral characterisation target will be shown and finally, the different spectral processing methods and evaluation metrics will be presented.

A. Hyperspectral Medical Systems

Several medical HS systems, customized for various applications (gynaecology (G_VNIR) [20], [21], histology (H_VNIR) [22], [23], [24], and neurosurgery (N_VNIR and N_NIR) [25], [26]) are going to be used in this study. Table I provides a summary of the medical HS systems, their integrated HS camera, and their key optical features.

TABLE I SUMMARY OF MEDICAL HS SYSTEMS

	G_VNIR	H_VNIR	N_VNIR	N_NIR
Application	Gynaecology	Histology	Neurosurgery	Neurosurgery
Optical System	Colposcope OP-C5 (OPTOMIC ESPAÑA, S.A., Spain)	Microscope Olympus BX53 (OLYMPUS Corp., Tokyo, Japan)	Custom	Custom
HS Camera	SnapScan VNIR	Pushbroom VNIR	Pushbroom VNIR	Pushbroom NIR
Magnification	0.4×, 0.6×, 1×, 1.6×, 2.5×	5×, 10×, 20× and 50×	1×	1×
Halogen Lamp Power (W)	50	100	150	150

More information about the HS sensor employed by each medical HS system is available in Table II. These setups are shown in Fig. 1. In addition, it must be mentioned that, for each medical HS system, custom software was developed to set image acquisition parameters.

TABLE II SUMMARY OF HS CAMERAS

	SnapScan VNIR	**Pushbroom VNIR**	**Pushbroom NIR**
HS Camera	Imec SNAPSCAN VNIR (Imec, Leuven, Belgium)	Hyperspec® VNIR A-Series, (Headwall Photonics, Inc., MA, USA)	Hyperspec® NIR 100/U, (Headwall Photonics, Inc., MA, USA)
HS Technology	SnapScan	Pushbroom	Pushbroom
Sensor	CMOS sensor, ams CMV2000 (ams OSRAM AG, Munich, Germany)	CCD sensor, Adimec-1000m (Adimec Advanced Image Systems B.V., Eindhoven, Netherlands)	InGaAs sensor, Xeneth XEVA 5052 (Xenics nv, Leuven, Belgium)
Spectral range (nm)	470 - 900	400 - 1000	900–1700
Spectral Sampling (nm)	2.86	0.72	4.65
Spectral Bandwidth / FWHM (nm)	10-15	2.5	4
# Spectral Channels	158	826	172
FOV (pixels)	1000 x 900	1×1004	1×320
Pixel Size (µm)	5.5	7.4	4.8

*CMOS: complementary metal-oxide semiconductor. CCD: charge-coupled device. InGaAs: Indium gallium arsenide. FOV: Field of View.

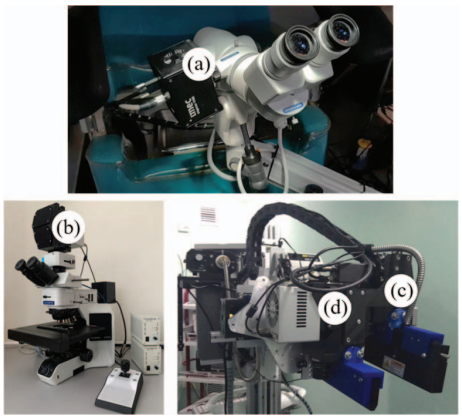

Fig. 1. Set-ups: (a) G_VNIR, (b) H_VNIR, (c) N_VNIR, and (d) N_NIR.

B. Spectral Characterization Target

The spectral characterization target which is going to be employed in this study is the NIST (National Institute of Standards and Technology) traceable wavelength calibration standard, which is composed by a mixture of three pure, rare-earth oxides (holmium, erbium, and dysprosium), mixed into Zenith Polymer® (LabSphere, Inc., NH, USA). The wavelength reference polymer exhibits distinct absorption peaks which provides a stable wavelength reference standard for validating spectrophotometers data. In Fig. 2 (a) it can be seen an image of the polymer itself which was captured once by each of the medical HS systems generating HS cubes of different sizes (G_VNIR (captured at 0.6×): 900×1000×158, H_VNIR (captured at 10×): 100×1004×826, N_VNIR: 741×1004×826, and N_NIR: 253×320×172). Fig. 2 (b) displays the spectral wavelength provided by the manufacturer (250 to 2450 nm, 2200 bands at 0.1 nm spectral resolution).

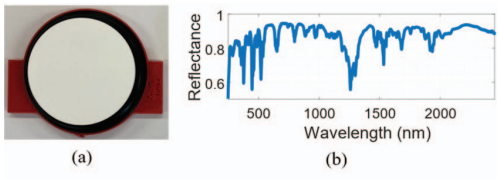

Fig. 2. Wavelength reference standard (a) picture and (b) spectral signature.

C. Processing Methods

During processing of HSI data, first flat-field correction is performed over the data to address variations caused by sensor and environmental factors [27]. This involves transforming digital numbers into radiation intensity [28] or true reflectance values [29], [30], [31]. The processes to convert raw sensor data (R) into calibrated images (CI), indicated in equation (1), requires a dark current (DC) capture, acquired with the shutter closed, and a white reference (WR), obtained using a diffuse reflectance standard from SphereOptics, which is produced using a Zenith Polymer® (LabSphere Inc., NH, USA) reflectance material [32]. This material is based on polytetrafluoroethylene and ensures a reflectivity above 99 %, making it an excellent choice for reflectance standards as it can withstand high levels of heat, humidity, and radiation exposure. These standards have a matte Lambertian reflecting surface, ensuring nearly equal intensity in all directions, with total reflection close to 100 % [32].

$$CI = \frac{R - DC}{WR - DC} \tag{1}$$

Flat-field correction is a well-established initial step before any further HSI processing [29], [30], [31], [33], [34]. However, further processing is subjected to the HSI instrumentation and data being studied. State-of-the-art HSI processing algorithms can be divided into smoothing, normalization, and spectral derivatives. Additionally, as emphasized by Rinnan *et al.* [6], the common practice involves combining processing techniques, with recommendations suggesting smoothing preceding normalization.

a. Smoothing Algorithms

Smoothing algorithms, aiming at reducing noise and irregularities, are conducted in the spectral domain of the data. These algorithms consider a symmetric window comprising k neighbours to the right- and left-hand side of a certain sample in the data sequence. All these values together comprise a smoothing window of odd value W, defined by (2). Since the signal at each point is affected by its neighbours' values, smoothing algorithms help to enhance signal and mitigate fluctuations, making patterns or trends more discernible but

attenuating high-frequency characteristics. The most common smoothing algorithms were selected for this study (Table III), where each algorithm is applied over a single spatial pixel R, producing a smoothed spectrum R_S . $\boldsymbol{\lambda}$ symbolizes the wavelength parameter.

$$W = 2k + 1; k \in \mathbb{N} \quad (2)$$

TABLE III SMOOTHING ALGORITHMS SUMMARY

Name	Acronym	Equation ($\boldsymbol{R_S(\lambda)}$)	Description
Average	MOVMEAN	$\frac{1}{W}\sum_{i=-k}^{k} R(\lambda + i\,\Delta\lambda)$	Mean value over a window to preserve the central tendency of the data.
Median	MOVMEDIAN	$Median$	Median value over a window to preserve the central tendency of the data when outliers are present.
Gaussian-weighted average	GAUSSIAN	$\frac{\sum_{i=-k}^{k} w_i\, R(\lambda + i\,\Delta\lambda)}{\sum_{i=-k}^{k} w_i}$	Gaussian-shaped weights (w_i), with standard deviation set to $W/5$, emphasizing points closer to the centre of the window.
Linear regression [35]	LOWESS	$\sum_{n=1}^{N} \beta_n R(\lambda)^n + \epsilon$ $\beta_n \equiv regression\ coefficients$ $\epsilon \equiv residuals$	First degree polynomial fitting ($N = 1$).
Quadratic regression [36]	LOESS		Second degree polynomial fitting ($N = 2$).
Robust linear regression [37]	RLOWESS		Modifies LOWESS by iteratively adjusting the weights to give less influence on outliers in the regression ($N = 1$).
Robust Quadratic regression [37]	RLOESS		Modifies LOESS by iteratively adjusting the weights to give less influence on outliers in the regression ($N = 2$).
Savitzky-Golay filter [38]	SGOLAY	$\frac{1}{F}\sum_{i=-k}^{k} C_i R(\lambda + i\,\Delta\lambda)$	Least squares fit via quadratic convoluting integers (C_i) and normalizing factor (F).

b. Normalization Algorithms

Normalization methods are employed in HSI to standardize data across its spectral component, ensuring comparability and removing biases caused by scale differences. The six normalization methods chosen for this work were the ones provided by Witteveen *et al* [16] in their review. They are further explained in (Table IV). Each algorithm is applied over a single spatial pixel R , producing a normalized spectrum R_N . $\boldsymbol{\lambda}$ symbolizes the wavelength parameter.

TABLE IV. NORMALIZATION ALGORITHMS SUMMARY

Name	Acronym	Equation ($\boldsymbol{R_N(\lambda)}$)	Description
Standard normal variate[39]	SNV	$\frac{R(\lambda) - \bar{R}}{\sigma}$	Each spectrum is subtracted its own arithmetic mean ($\bar{R}$) and divided by the unbiased estimation of its standard deviation (σ).
Multiplicative scatter correction [40], [41]	MSC	$\frac{R_i(\lambda) - c}{d}$ $R_i(\lambda) = c + d \cdot \bar{R};$	Each spectrum is scaled and offset to fit a reference (mean spectrum).
Min-max Normalization	MINMAX	$\frac{R(\lambda) - \min(R(\lambda))}{\max(R(\lambda)) - \min(R(\lambda))}$	Each spectrum is scaled and offset using its min and max values.
Mean centering	MC	$R(\lambda) - \bar{R}$	Each spectrum is subtracted its own mean.
Single wavelength	SW	$\frac{R(\lambda)}{R(\lambda_0)}$ $\lambda_0 = \arg\max(R(\lambda))$	Each spectrum is divided by its value at the reference wavelength with most reflectance (λ_0).
Area Under the Curve	AUC	$\frac{R(\lambda)}{\sum_{\lambda=1}^{\lambda_{end}} R(\lambda)}$	Each spectrum is divided by its AUC.

c. Spectral Derivatives Algorithms

Finally, spectral derivative algorithms analyse changes in spectral data, revealing variations in absorption, reflectance, or emission properties across wavelengths. The specificity of absorption ranges of human molecules, as noted by Steven Jaques [REF], typically contains crucial information for distinguishing tissues. However, detecting small peaks can be challenging. In this sense, derivative methods, are crucial for identifying subtle spectral features and patterns not readily apparent in calibrated data. For this preliminary study, just the first and second derivatives were assessed for simplicity. They are detailed in Table V, where $R_D(\lambda)$ is the value of the derived spectrum at that λ.

TABLE V DERIVATIVES ALGORITHS SUMMARY

Name	Acronym	Equation ($\boldsymbol{R_D(\lambda)}$)	Description
First derivative	FD	$\frac{R(\lambda + \Delta\lambda) - R(\lambda)}{\Delta\lambda}$	Approximation of the first derivative of each spectrum from first differences.
Second derivative	SD	$\frac{R(\lambda + 2\,\Delta\lambda) - R(\lambda)}{(\Delta\lambda)^2}$	Approximation of the second derivative of each spectrum from second differences.

D. Evaluation Metrics

After calculating the different processing over the calibrated data, evaluation metrics are needed to assess the similarity between the pre-processed data and the wavelength reference standard. Additionally, execution time is measured to compare their overall performance.

a. RMSE

RMSE is a statistical measure that assesses the accuracy of a model by quantifying the differences between observed (O_i) and actual (A_i) values, as described in (3), where N is the common size of both, the observed and the actual sequences. A lower RMSE value, close to zero, indicates a stronger similarity between the spectral signatures.

$$RMSE = \sqrt{\frac{1}{N}\sum_{i=1}^{N}(O_i - A_i)^2} \quad (3)$$

The methodology followed in this work includes the evaluation of pre-processed HS data against a wavelength reflectance standard. In terms of smoothing algorithms, it must

be considered that its aim is to reduce local noise while keeping main features of the signal intact. Thus, when evaluating spectral signatures pre-processed using a smoothing algorithm, the data is compared to the wavelength reflectance standard. Since in normalization and spectral derivative methods the HS data undergoes a transformation that alters its offset and scale, their inverse operation is applied over the pre-processed data relative to the wavelength reflectance standard. For instance, in the case of the MC normalization method, following the subtraction of each spectrum's individual mean, the average value of the wavelength reflectance standard is added back to all spectra.

b. Execution Time

To determine the execution time of each algorithm in MATLAB® 2023a, the processing algorithms will be timed 10,000 times across a dataset composed of 10 pixel-wise spectra of 3095 bands each. The processing methods was executed on an Intel(R) Core (TM) i7-10700K processor with 64 GB of RAM.

III. Results and Discussion

In this section, the reflectance data will be shown. Several processing methods are applied over the HS data, which are then compared to the wavelength reflectance standard.

A. Flat-field Correction

Flat-field correction was carried out over the captured HS data to compensate for variations due to sensor and environmental factors. This process involved converting digital numbers into radiation intensity or true reflectance values. Then, extreme bands were removed for each sensor, since they exhibit a low signal to noise ratio. In the H_VNIR and N_VNIR systems, since they use the same HS camera, the same spectral range was removed (400- 440 and 909-1000 nm), resulting two HS cubes composed by 645 spectral bands each. The HS cubes of N_NIR system were composed of 144 spectral bands, removing the 900-956 and 1638-1700 nm spectral range. Finally, a registration of the wavelength reflectance standard with the HS data of each setup was performed by selecting the closets values of the standard wavelength vector with respect to the one of each setup (mean produced error was 0.025 nm).

Fig. 3 illustrates, for each setup, one calibrated spectral signature and its registered wavelength reference standard. It is important to note that the wavelength calibration standard is made of is a mixture of three pure, rare-earth oxides (Holmium, Erbium and Dysprosium) mixed into Zenith Polymer®. Whereas the SphereOptics white reference exhibits diffused reflection, light can be specular reflected in the small crystals of the rare-earth polymer, resulting in higher values on the raw HS cube compared to those in the white reference. This effect can cause the calibrated cube to have values above one, as seen in Fig. 3 (a), (b) and (c). Other wavelengths calibration standards will be explored in future experiments.

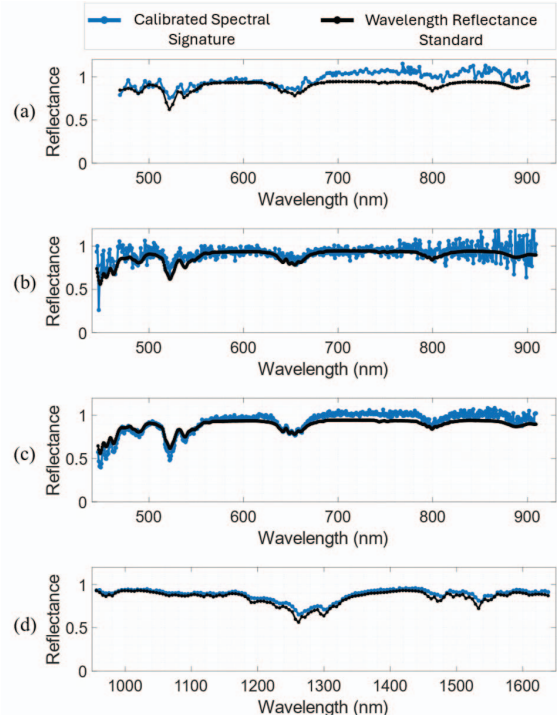

Fig. 3. Calibrated spectral signature of the different medical HS systems (blue), and the registered wavelength reference standard (black): (a) G_VNIR, (b) H_VNIR, (c) N_VNIR, and (d) N_NIR.

B. Processing Methods

a. Smoothing Algorithms

Smoothed pre-processed data from different setups were compared to the wavelength reflectance standard to find a smoothing method that balances the reduction of high-frequency noise and the retention of significant data. Smoothing was performed using a prescribed number of neighbours, 7, which resulted in window sizes of 20.02 nm for G_VNIR, 5.04 nm in H_VNIR and N_VNIR, and 32.55 nm in N_NIR (see Table II). These differences explain the dependency of results on the particular HS sensor used, as shown in Fig. 4 (a). H_VNIR and N_VNIR systems use the same pushbroom VNIR camera, and so their most effective algorithm correlates (MOVEMEAN). For the other two medical HS systems, GAUSSIAN algorithm works best for G_VNIR and LOESS for N_NIR. This last medical HS system consistently yields the best results, possibly due to its larger spectral sampling, since a wider spectral window is being considered when smoothing. Conversely, the H_VNIR system exhibits the opposite behaviour. This discrepancy suggests that the optimal smoothing algorithms and window sizes may need to be customized for different medical HSI systems. Furthermore, RMSE values of the unprocessed data with respect to the wavelength reflectance standard are also given for comparison (REF in Fig. 4 (a)). In terms of execution times (Fig. 4 (b)), it must be considered that RLOWESS and RLOESS have significantly longer execution times (~ 40.000 s) compared to others (~ 0.050 s), making the former ones less desirable. Also, it should be noted that MOVEMEAN is the fastest (0.035 s) since it is the simplest one.

Fig. 4. Smoothing processing methods evaluation: (a) RMSE and (b) execution times. * represents the best values for each HS system.

b. Normalization Algorithms

Several normalization algorithms have been also examined, ranging from simple subtraction (MC) or scaling (AUC, SW) to combinations of these methods (SNV, MSC, MM). Results in Fig. 5 (a), indicate that SNV algorithm outperforms other normalization methods across all setups. The SNV algorithm is one of the combined methods that brings the pre-processed HS data closer to the wavelength reflectance standard. This algorithm becomes useful for uniform samples, but it should be further studied in real-world scenarios. Moreover, it can be observed that reference RMSE values of the unprocessed data with respect to the wavelength reflectance standard (REF in Fig. 5 (a)) are clearly improved using all methods but SW. Regarding execution times (Fig. 5 (b)), all algorithms take approximately 0.002 to 0.054 s. However, MSC is in the upper time bound, as it requires the fitting of a polynomial for each data point. The rest of the methodologies, based on basic operations, show no significant differences in their execution times.

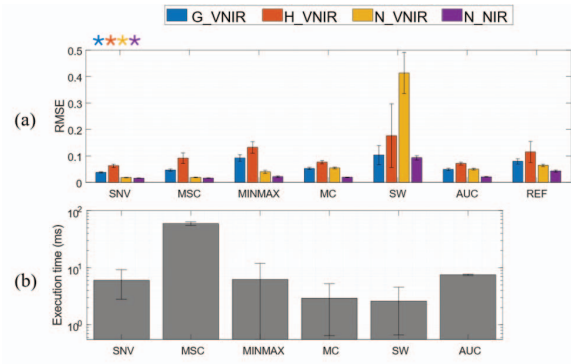

Fig. 5. Normalization processing methods evaluation: (a) RMSE and (b) execution times. * represents the best values for each HS system.

c. Spectral Derivatives Algorithms

Spectral derivative algorithms were also examined as an extra step of the processing chain. It is crucial to note that these methods are highly sensitive to noise, thus they must be applied to data that have already undergone noise reduction. Since MOVMEAN and SNV were the best performing algorithms, they are selected as the initial step before applying spectral derivatives. Results of comparing spectral derivate HS data with respect to the wavelength reflectance standard are shown in Fig. 6 (a). RMSE values show that FD performed better than the SD, although, not better than evaluating the unprocessed data with respect to the wavelength reflectance standard (REF in Fig. 6 (a)). This could be attributed to noise in the data. While derivatives are essential for identifying subtle spectral features and patterns that are not easily visible in calibrated data, they also amplify noise peaks. In terms of execution times (Fig. 6 (b)), SD algorithm is slower since it is composed of two FD in series.

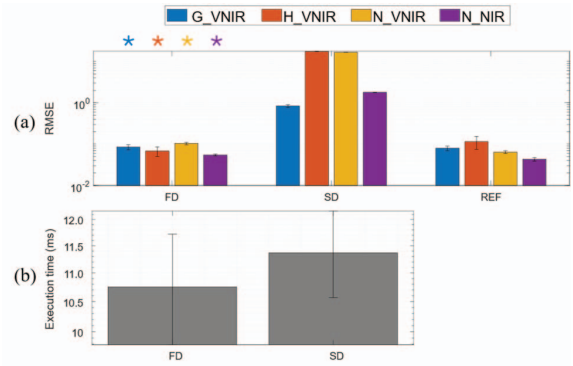

Fig. 6. Derivatives spectral processing methods evaluation: (a) RMSE and (b) execution times.* represents the best values for each HS system.

d. Combination of Algorithms

Furthermore, as recommended by Rinnan *et al.* [6], combining various processing algorithms is advisable, specifically suggesting smoothing prior to normalization. Following this guidance, all normalization algorithms were tested after applying each smoothing algorithm to the HS data, resulting in a total of 48 combinations. Table VI presents the RMSE values for each medical HS system, detailing the results for optimal smoothing, normalization, their combination, and the additional step of applying spectral derivative methods.

TABLE VI. RMSE OF BEST PERFORMING PROCESSING ALGORITHMS

	G_VNIR	H_VNIR	N_VNIR	N_NIR
Smoothing	GAUSSIAN	MOVMEAN	MOVMEAN	LOESS
	0.075	0.091	0.061	0.043
Normalization	SNV			
	0.037	0.063	0.018	0.016
Smoothing + Normalization	**SGOLAY + SNV**	**MOVMEAN + SNV**	**GAUSSIAN + SNV**	**LOESS + SNV**
	0.035	**0.036**	**0.015**	**0.015**
Smoothing + Normalization + Spectral Derivative	MOVMEAN + SNV + FD			
	0.045	0.077	0.0423	0. 0432

Although there is a consensus on the best normalization method (SNV), results show discrepancies in the best smoothing algorithms when applied alone versus in combination with normalization. This is due to the small differences between methods (~0.001). Additionally, applying derivatives to the data does not improve the evaluation results. Fig. 7 illustrates, for

each medical HS system, the processed data providing the best results (their best smoothing following by SNV normalization without the further step of derivatives). The calibrated and reference data are also provided for qualitatively evaluation. It can be observed how after the processing step, the H_VNIR data still shows high levels of noise, contrasting with the notably improved performance of G_VNIR and N_NIR data. This might be due to the lower spectral sampling of the pushbroom VNIR sensor, as the window size is not optimized to effectively reduce its high-frequency noise peaks. Further analysis is required to optimize the window size, adapting it to different spectral sampling sensors.

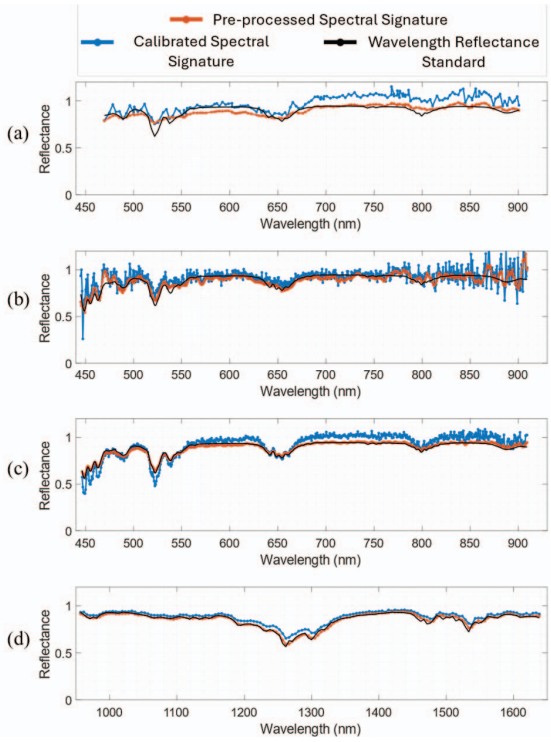

Fig. 7. Best pre-processed, smooth and normalized, spectral signature (orange) for each medical HS system, calibrated spectral signatures (blue) and wavelength reflectance standard (black): (a) G_VNIR, (b) H_VNIR, (c) N_VNIR, and (d) N_NIR.

IV. Conclusion

In this study, the need for effective processing methods in medical HSI data was addressed. The innovation lies in the generic optimization of spectral processing methods using a wavelength reflectance standard, instead of analysing a dataset for a specific application. The objective was to evaluate processing techniques to enhance spectral data quality and reliability by reducing noise and unwanted artifacts. First, a review of the state-of-the-art was performed, and various processing algorithms, focusing on smoothing, normalization, and spectral derivatives, were identified. Then, a wavelength reference standard was captured using four medical HS systems (G_VNIR, H_VNIR, N_VNIR and N_NIR). Each processing method was applied to the data recorded by the different medical HS systems. The performance of these processing methods was assessed using RMSE to compare processed data with the wavelength reference standard, and the execution time of each algorithm was considered to assess practical feasibility and efficiency.

Results highlight the effectiveness of certain processing techniques for each medical HS system. In terms of smoothing, the algorithms giving the best results were GAUSSIAN for G_VNIR, MOVMEDIAN for H_VNIR and N_VNIR and LOESS for N_NIR. The choice of smoothing algorithm varies across setups because of the different spectral sampling of HS camera employed. In terms of normalization, the SNV algorithm delivers optimal results across all medical HS systems, since it normalizes the scale and offset of the captured HS data which makes it more similar to the reference than the other algorithms. Furthermore, combining smoothing and normalization methods enhances performance, although different results are obtained for each medical HS system due to the non-optimized window size. Lastly, concerning spectral derivatives, FD performs better than SD, although none of them improves previous results since they enlarge the noise present on the data.

Regarding execution times, most algorithms are executed within the range of 10^{-2} to 10^{-3} s. However, RLOWESS and RLOESS, characterized as slow smoothing algorithms, exhibit longer processing times (~ 40 s). Nevertheless, future work will focus on analysing the performance of these algorithms on GPU or FPGA platforms in order to improve the algorithm performance, targeting real-time applications. Thus, the times obtained in different platforms allow to compare the proposed solutions against each other while providing a guideline for estimating the time required to process a given amount of data and for determining the appropriate algorithm for any particular application.

Despite the promising outcomes observed, our study has several limitations that require further attention. Concerning smoothing algorithms, optimizing the window size for noise reduction is necessary. Additionally, other processing algorithms should be considered to address spectral misalignment. Additionally, it is essential to acknowledge that the selection of evaluation metrics and benchmark datasets may impact result interpretation. Hence, further analysis using actual captured data is necessary to apply our findings to real-world HSI scenarios with increased complexity and variability.

Acknowledgment

This work was developed while Laura Quintana-Quintana, Carlos Vega, and Raquel Leon were beneficiaries of the pre-doctoral grant given by the "Agencia Canaria de Investigacion, Innovacion y Sociedad de la Información (ACIISI)" of the "Consejería de Economía, Conocimiento y Empleo", which is part-financed by the European Social Fund (FSE) (POC 2014-2020, Eje 3 Tema Prioritario 74 (85 %)). Moreover, this work is part of the TALENT (HypErsPEctRal Imaging for Artificial intelligence applications) project (PID2020-116417RB-C41), supported by the Spanish Government and European Union (FEDER Funds). This work has also been partially developed under the STRATUM project which received funding from the European Union's Horizon Europe Programme HORIZON-IA action under grant agreement No. 101137416.

REFERENCES

[1] F. D. van der Meer *et al.*, "Multi- and hyperspectral geologic remote sensing: A review," *International Journal of Applied Earth Observation and Geoinformation*, vol. 14, no. 1, pp. 112–128, Feb. 2012, doi: 10.1016/j.jag.2011.08.002.

[2] E. Kho, B. Dashtbozorg, L. L. de Boer, K. K. Van de Vijver, H. J. C. M. Sterenborg, and T. J. M. Ruers, "Broadband hyperspectral imaging for breast tumor detection using spectral and spatial information," *Biomed Opt Express*, vol. 10, no. 9, p. 4496, Sep. 2019.

[3] S. Ortega, H. Fabelo, R. Camacho, M. de la Luz Plaza, G. M. Callicó, and R. Sarmiento, "Detecting brain tumor in pathological slides using hyperspectral imaging," *Biomed Opt Express*, vol. 9, no. 2, p. 818, Feb. 2018, doi: 10.1364/BOE.9.000818.

[4] T. Collins *et al.*, "Automatic Recognition of Colon and Esophagogastric Cancer with Machine Learning and Hyperspectral Imaging," *Diagnostics*, vol. 11, no. 10, p. 1810, Sep. 2021, doi: 10.3390/diagnostics11101810.

[5] L. A. Zherdeva *et al.*, "Hyperspectral imaging of skin and lung cancers," J. Popp, V. V. Tuchin, D. L. Matthews, and F. S. Pavone, Eds., Apr. 2016, p. 98870S. doi: 10.1117/12.2227602.

[6] Åsmund Rinnan, F. van den Berg, and S. B. Engelsen, "Review of the most common pre-processing techniques for near-infrared spectra," *TrAC Trends in Analytical Chemistry*, vol. 28, no. 10, pp. 1201–1222, Nov. 2009, doi: 10.1016/j.trac.2009.07.007.

[7] J. Engel *et al.*, "Breaking with trends in pre-processing?," *TrAC Trends in Analytical Chemistry*, vol. 50, pp. 96–106, Oct. 2013, doi: 10.1016/j.trac.2013.04.015.

[8] J. Ezenarro, D. Schorn-García, O. Busto, and R. Boqué, "ProSpecTool: A MATLAB toolbox for spectral preprocessing selection," *Chemometrics and Intelligent Laboratory Systems*, vol. 247, p. 105096, Apr. 2024, doi: 10.1016/j.chemolab.2024.105096.

[9] I. Ruisánchez *et al.*, "Preliminary results of an interlaboratory study of chemometric software and methods on NIR data. Predicting the content of crude protein and water in forages," *Chemometrics and Intelligent Laboratory Systems*, vol. 63, no. 2, pp. 93–105, 2002, doi: https://doi.org/10.1016/S0169-7439(02)00039-4.

[10] D. Cozzolino, P. J. Williams, and L. C. Hoffman, "An overview of pre-processing methods available for hyperspectral imaging applications," *Microchemical Journal*, vol. 193, p. 109129, Oct. 2023, doi: 10.1016/j.microc.2023.109129.

[11] S. Singh and S. S. Kasana, "A Pre-processing framework for spectral classification of hyperspectral images," *Multimed Tools Appl*, vol. 80, no. 1, pp. 243–261, Jan. 2021, doi: 10.1007/s11042-020-09180-2.

[12] I. T. Jolliffe and J. Cadima, "Principal component analysis: a review and recent developments," *Philosophical Transactions of the Royal Society A: Mathematical, Physical and Engineering Sciences*, vol. 374, no. 2065, p. 20150202, Apr. 2016, doi: 10.1098/rsta.2015.0202.

[13] D. B. Bhushan, V. Sowmya, M. S. Manikandan, and K. P. Soman, "An effective pre-processing algorithm for detecting noisy spectral bands in hyperspectral imagery," in *2011 International Symposium on Ocean Electronics*, 2011, pp. 34–39. doi: 10.1109/SYMPOL.2011.6170495.

[14] G. Vane, R. O. Green, T. G. Chrien, H. T. Enmark, E. G. Hansen, and W. M. Porter, "The airborne visible/infrared imaging spectrometer (AVIRIS)," *Remote Sens Environ*, vol. 44, no. 2–3, pp. 127–143, May 1993, doi: 10.1016/0034-4257(93)90012-M.

[15] R. Koprowski, "Hyperspectral imaging in medicine: image pre-processing problems and solutions in Matlab," *J Biophotonics*, vol. 8, no. 11–12, pp. 935–943, Nov. 2015, doi: 10.1002/jbio.201400133.

[16] M. Witteveen, H. J. C. M. Sterenborg, T. G. van Leeuwen, M. C. G. Aalders, T. J. M. Ruers, and A. L. Post, "Comparison of preprocessing techniques to reduce nontissue-related variations in hyperspectral reflectance imaging," *J Biomed Opt*, vol. 27, no. 10, Oct. 2022, doi: 10.1117/1.JBO.27.10.106003.

[17] E. Kho *et al.*, "Feasibility of Ex Vivo Margin Assessment with Hyperspectral Imaging during Breast-Conserving Surgery: From Imaging Tissue Slices to Imaging Lumpectomy Specimen," *Applied Sciences*, vol. 11, no. 19, 2021, doi: 10.3390/app11198881.

[18] E. J. M. Baltussen *et al.*, "Hyperspectral imaging for tissue classification, a way toward smart laparoscopic colorectal surgery," *J Biomed Opt*, vol. 24, no. 01, p. 1, Jan. 2019, doi: 10.1117/1.JBO.24.1.016002.

[19] E. Kho *et al.*, "Hyperspectral Imaging for Resection Margin Assessment during Cancer Surgery," *Clinical Cancer Research*, vol. 25, no. 12, pp. 3572–3580, Jun. 2019, doi: 10.1158/1078-0432.CCR-18-2089.

[20] C. Vega *et al.*, "Development of a Hyperspectral Colposcope for Early Detection and Assessment of Cervical Dysplasia," in *2022 25th Euromicro Conference on Digital System Design (DSD)*, IEEE, Aug. 2022, pp. 863–870. doi: 10.1109/DSD57027.2022.00121.

[21] C. Vega García *et al.*, "Feasibility Study of Hyperspectral Colposcopy as a Novel Tool for Detecting Precancerous Cervical Lesions." May 2024. doi: 10.21203/rs.3.rs-4343232/v1.

[22] S. Ortega *et al.*, "Hyperspectral Superpixel-Wise Glioblastoma Tumor Detection in Histological Samples," *Applied Sciences*, vol. 10, no. 13, p. 4448, Jun. 2020, doi: 10.3390/app10134448.

[23] S. Ortega *et al.*, "Hyperspectral Imaging for the Detection of Glioblastoma Tumor Cells in H&E Slides Using Convolutional Neural Networks," *Sensors*, vol. 20, no. 7, p. 1911, Mar. 2020, doi: 10.3390/s20071911.

[24] L. Quintana-Quintana, S. Ortega, H. Fabelo, F. J. Balea-Fernández, and G. M. Callico, "Blur-specific image quality assessment of microscopic hyperspectral images," *Opt Express*, vol. 31, no. 8, p. 12261, Apr. 2023, doi: 10.1364/OE.476949.

[25] R. Leon *et al.*, "Evaluation of Hyperspectral Imaging Fusion for in-vivo Brain Tumor Identification and Delineation," in *2023 26th Euromicro Conference on Digital System Design (DSD)*, IEEE, Sep. 2023, pp. 493–499. doi: 10.1109/DSD60849.2023.00074.

[26] R. Leon *et al.*, "VNIR–NIR hyperspectral imaging fusion targeting intraoperative brain cancer detection," *Sci Rep*, vol. 11, no. 1, p. 19696, Oct. 2021, doi: 10.1038/s41598-021-99220-0.

[27] B. Boldrini, W. Kessler, K. Rebner, and R. W. Kessler, "Hyperspectral Imaging: A Review of Best Practice, Performance and Pitfalls for in-line and on-line Applications," *J Near Infrared Spectrosc*, vol. 20, no. 5, pp. 483–508, Oct. 2012, doi: 10.1255/jnirs.1003.

[28] G. Yang *et al.*, "The DOM Generation and Precise Radiometric Calibration of a UAV-Mounted Miniature Snapshot Hyperspectral Imager," *Remote Sens (Basel)*, vol. 9, no. 7, p. 642, Jun. 2017, doi: 10.3390/rs9070642.

[29] P. Geladi, J. Burger, and T. Lestander, "Hyperspectral imaging: calibration problems and solutions," *Chemometrics and Intelligent Laboratory Systems*, vol. 72, no. 2, pp. 209–217, Jul. 2004, doi: 10.1016/j.chemolab.2004.01.023.

[30] D. Nouri, Y. Lucas, and S. Treuillet, "Calibration and test of a hyperspectral imaging prototype for intra-operative surgical assistance," M. N. Gurcan and A. Madabhushi, Eds., Mar. 2013, p. 86760P. doi: 10.1117/12.2006620.

[31] A. Noviyanto and W. H. Abdulla, "Segmentation and calibration of hyperspectral imaging for honey analysis," *Comput Electron Agric*, vol. 159, pp. 129–139, Apr. 2019, doi: 10.1016/j.compag.2019.02.006.

[32] "Encapsulated Gray Scale Standards - Avian Technologies." Accessed: Jun. 03, 2021. [Online]. Available: https://aviantechnologies.com/product/encapsulated-gray-scale-standards/

[33] S. Ortega *et al.*, "Hyperspectral Push-Broom Microscope Development and Characterization," *IEEE Access*, vol. 7, pp. 122473–122491, 2019, doi: 10.1109/ACCESS.2019.2937729.

[34] L. Quintana *et al.*, "Instrumentation Evaluation for Hyperspectral Microscopy Targeting Enhanced Medical Histology," in *2021 XXXVI Conference on Design of Circuits and Integrated Systems (DCIS)*, IEEE, Nov. 2021, pp. 1–6. doi: 10.1109/DCIS53048.2021.9666188.

[35] W. S. Cleveland, "LOWESS: A Program for Smoothing Scatterplots by Robust Locally Weighted Regression," *Am Stat*, vol. 35, no. 1, p. 54, Feb. 1981, doi: 10.2307/2683591.

[36] W. S. Cleveland and S. J. Devlin, "Locally Weighted Regression: An Approach to Regression Analysis by Local Fitting," *J Am Stat Assoc*, vol. 83, no. 403, pp. 596–610, Sep. 1988, doi: 10.1080/01621459.1988.10478639.

[37] W. S. Cleveland, "Robust Locally Weighted Regression and Smoothing Scatterplots," *J Am Stat Assoc*, vol. 74, no. 368, pp. 829–836, Dec. 1979, doi: 10.1080/01621459.1979.10481038.

[38] Abraham. Savitzky and M. J. E. Golay, "Smoothing and Differentiation of Data by Simplified Least Squares Procedures.," *Anal Chem*, vol. 36, no. 8, pp. 1627–1639, Jul. 1964, doi: 10.1021/ac60214a047.

[39] R. J. Barnes, M. S. Dhanoa, and S. J. Lister, "Standard Normal Variate Transformation and De-Trending of Near-Infrared Diffuse Reflectance Spectra," *Appl Spectrosc*, vol. 43, no. 5, pp. 772–777, 1989, doi: 10.1366/0003702894202201.

[40] P. Geladi, D. MacDougall, and H. Martens, "Linearization and Scatter-Correction for Near-Infrared Reflectance Spectra of Meat," *Appl Spectrosc*, vol. 39, no. 3, pp. 491–500, May 1985, doi: 10.1366/0003702854248656.

[41] H. Martens, S. Jensen, and P. Geladi, "Multivariate Linearity Transformations for Near Infrared Reflectance Spectroscopy," *Applied Statistic*, pp. 205–234, 1983.